Pulsed hydrogen–deuterium exchange mass spectrometry probes conformational changes in amyloid beta (Aβ) peptide aggregation

Ying Zhang, Don L. Rempel, Jun Zhang, Anuj K. Sharma, Liviu M. Mirica[1], and Michael L. Gross[1]

Department of Chemistry, Washington University in St. Louis, St. Louis, MO 63130

Edited by Harry B. Gray, California Institute of Technology, Pasadena, CA, and approved July 23, 2013 (received for review May 14, 2013)

Probing the conformational changes of amyloid beta (Aβ) peptide aggregation is challenging owing to the vast heterogeneity of the resulting soluble aggregates. To investigate the formation of these aggregates in solution, we designed an MS-based biophysical approach and applied it to the formation of soluble aggregates of the $Aβ_{42}$ peptide, the proposed causative agent in Alzheimer's disease. The approach incorporates pulsed hydrogen–deuterium exchange coupled with MS analysis. The combined approach provides evidence for a self-catalyzed aggregation with a lag phase, as observed previously by fluorescence methods. Unlike those approaches, pulsed hydrogen–deuterium exchange does not require modified $Aβ_{42}$ (e.g., labeling with a fluorophore). Furthermore, the approach reveals that the center region of $Aβ_{42}$ is first to aggregate, followed by the C and N termini. We also found that the lag phase in the aggregation of soluble species is affected by temperature and Cu^{2+} ions. This MS approach has sufficient structural resolution to allow interrogation of Aβ aggregation in physiologically relevant environments. This platform should be generally useful for investigating the aggregation of other amyloid-forming proteins and neurotoxic soluble peptide aggregates.

soluble Aβ oligomers | amyloid beta peptide | copper | electrospray ionization | Finke–Watsky mode

Protein aggregation is one of the immediate causes of Alzheimer's, Parkinson, and Huntington diseases, motivating biophysical studies of the responsible proteins. More than 20 small proteins undergo amyloidosis in humans. In Alzheimer's disease (AD), the aggregation of the 40- or 42-aa-long amyloid beta (Aβ) peptide, generally called $Aβ_{40}$ or $Aβ_{42}$, respectively, is proposed to be involved in the onset of the disease (1, 2). $Aβ_{42}$ is more amyloidogenic and more neurotoxic than $Aβ_{40}$. Although the amyloid-cascade hypothesis suggests that the Aβ-containing amyloid plaques are responsible for neurodegeneration (3–7), other studies suggest that soluble aggregates of $Aβ_{42}$ are more neurotoxic than the amyloid plaques (8–13).

The amyloid plaques in AD-affected brains contain high levels of copper, zinc, and iron (14–20). Among these, Cu has drawn the most attention because the Aβ precursor protein is likely a Cu-chaperone protein (21). Several studies of Cu^{2+}–$Aβ_{40}$ interactions show that Cu^{2+} can promote $Aβ_{40}$ aggregation (14, 18, 19).

The structure of $Aβ_{42}$ and its aggregates, although studied extensively, remains of high interest. Studies of amyloid fibrils invoke X-ray crystallography (22–24), EM (19, 25, 26), and thioflavin T fluorescence (19, 27), revealing the polypeptide's global behavior, whereas NMR studies provide residue-level information for the fibrils (28–30). Nevertheless, we know little about soluble Aβ aggregates owing to their intrinsically high heterogeneity.

MS should offer an opportunity for investigating soluble aggregates of $Aβ_{42}$. Thus far, there are no MS-based, time-dependent studies of the formation of soluble aggregates. Moreover, there are no other biophysical studies of $Aβ_{42}$ aggregation at the peptide (regional) level. MS, however, was used for analyzing the aggregated Aβ fibrils (31–33) and, with ion mobility (34–36), for soluble Aβ aggregates. Hydrogen–deuterium exchange (HDX) (37–42), even with top-down sequencing, can afford residue-level information (43, 44) and provide insight on $Aβ_{42}$ fibril core structure (31, 32) and its recycling (33, 45).

In light of the dearth of aggregation studies at the peptide level, we have used herein pulsed HDX to study the aggregation of the $Aβ_{40}$ and $Aβ_{42}$ peptides. Our platform is suitable for confirming the effect of temperature, agitation, and presence of Cu^{2+} ions on Aβ aggregation. Pulsed HDX, developed by Englander and coworkers (46), can be used for detecting protein folding intermediates (47) and membrane protein behavior (48). Others have also applied pulsed HDX to analyze fibril (33) and oligomer (43, 44) Aβ structures. To explain the experimental data, we used a self-catalyzed aggregation model, and its success suggests utility for other amyloid-forming proteins.

Materials and Methods

Protein Preparation. A synthetic, wild-type human form of $Aβ_{40}$ (Keck Biotechnology Resource Laboratory) and a recombinant, wild-type human form of $Aβ_{42}$ (rPeptide) were used. Sample preparation followed a reported procedure (49) as detailed in *Supporting Information*. Aβ films were thawed and dissolved in dry DMSO at 1 mM before aggregation. Aβ aggregation studies were initiated by diluting 1:19 (vol/vol) monomeric Aβ (either $Aβ_{40}$ or $Aβ_{42}$) into PBS buffer (pH 7.4) at 25 °C. Aggregation was allowed to occur over various incubation times ranging from 1 min to 48 h and under various experimental conditions as described in *Supporting Information*. Native gel electrophoresis and Western blotting were conducted as previously described (19).

Pulsed HDX. HDX experiments were carried out by mixing the incubated protein sample with D_2O buffer in a 1:1 (vol/vol) ratio (pulsed labeling for 1 min at 0 °C). HDX was then quenched by mixing the exchanging solution with 30 μL 3 M urea and 1% TFA to give a pH of 2.5. Pepsin digestion of Aβ and data analysis and processing (50) were used as described in *Supporting Information*. Importantly, the HDX time was fixed for each experiment, so the term "time" hereafter means aggregation time unless stated otherwise.

Finke–Watzky Modeling. The experimentally determined time-dependent data (mass shift vs. incubation time) were characterized phenomenologically by following the recommendation of Finke and coworkers (51) to use the simplest model consistent with the data. A bootstrap resampling method (52–54) was then used to evaluate the uncertainty of $t_{1/2}$ (*Supporting Information* gives details).

Results and Discussion

Our goal is to implement a general MS approach to monitor Aβ aggregation under different incubation conditions. Both HDX and aggregation are time-dependent phenomena. To minimize

Author contributions: L.M.M. and M.L.G. designed research; Y.Z. and A.K.S. performed research; Y.Z., D.L.R., J.Z., and A.K.S. analyzed data; and Y.Z., L.M.M., and M.L.G. wrote the paper.

The authors declare no conflict of interest.

This article is a PNAS Direct Submission.

[1]To whom correspondence may be addressed. E-mail: mirica@wustl.edu or mgross@wustl.edu.

This article contains supporting information online at www.pnas.org/lookup/suppl/doi:10.1073/pnas.1309175110/-/DCSupplemental.

aggregation during HDX and thereby separate aggregation and HDX, we used pulsed HDX whereby we allowed Aβ to incubate for various times and then submitted the mixture to a rapid pulsed HDX (1 min) followed by the usual quench procedure. Before MS analysis, we centrifuged the sample, split it into two equal parts representing the top and bottom parts, respectively, and analyzed the latter aliquot that is enriched in Aβ oligomers and aggregates.

Comparison of $A\beta_{42}$ and $A\beta_{40}$ Aggregation by Native Gel and Western Blotting. After various aggregation times, we analyzed the $A\beta_{40}$ and $A\beta_{42}$ samples by native gel and Western blotting to permit an accurate comparison of the aggregated species (Fig. S1). We found that the top half of the solution after centrifugation showed no detectable aggregates but only Aβ monomer, indicating that most of the monomer is homogeneously distributed, whereas larger soluble species move to the bottom half. We used the $A\beta_{40}$ peptide as a control, which showed only the presence of $A\beta_{40}$ monomer in all of the "bottom-half" samples (Fig. S1, *a–c*), in agreement with previous work (55). $A\beta_{42}$, however, showed a quite different behavior. After only 1 min of incubation, formation of low-molecular-weight (LMW) $A\beta_{42}$ oligomers (i.e., mostly trimer and tetramer) was observed. With longer incubation time, high-molecular-weight (HMW) soluble $A\beta_{42}$ oligomers in the 50- to 110-kDa range were observed. The amyloid fibrils, which are too large to enter the gel, were observed at the top of gel lanes. All these results are consistent with previously published work showing that $A\beta_{42}$ has a greater tendency to form aggregates than $A\beta_{40}$ (34, 55).

Pulsed HDX Analysis of Soluble Aβ Species. To conduct a more detailed characterization of various regions of Aβ, we applied pepsin proteolysis following the pulsed HDX treatment described above. Because most of the soluble Aβ species were on the bottom-half fraction upon centrifugation, we performed all analyses on the bottom-half solution. Seven peptides were observed: the N-terminus region (1–19 and 4–19), middle region (20–33, 20–34, and 20–35), and C-terminus region (35–40/42 and 36–40/42). We used three of these peptides (i.e., 1–19, 20–35, and 36–40/42) to analyze the HDX results because these fragments provide full Aβ coverage.

The pulsed HDX approach used to probe the Aβ aggregation states as a function of incubation time is unlike most HDX protocols, in which the protein is incubated in D_2O buffer for various times, quenched, and analyzed. Here the HDX time is a short (1 min) "pulse" after various incubation times. This pulse time is sufficient to allow the maximum exchange for this largely intrinsically disordered protein yet is negligible compared with the incubation times. We view this pulsed HDX as a "recording" tool to monitor aggregation without competing with it, allowing us to separate experimentally the aggregation from HDX.

Initially, we followed the aggregation of $A\beta_{40}$ at 25 °C by pulsed HDX as a control experiment (Fig. 1). All three peptic peptides monitored show a constant HDX extent as a function of incubation time. This indicates that no detectable conformational changes or self-association occurred from 1 min to 48 h at 25 °C. The apparent protection is likely due to two factors: (*i*) The exchange time is sufficiently short for the pulse (1 min) that HDX is not complete and (*ii*) there is significant back-exchange for the highly disordered $A\beta_{40}$ (*Supporting Information*). This extent of HDX is consistent not only with our native gel and Western blotting experiments, but also with the common perception that $A\beta_{40}$ forms fewer aggregates than $A\beta_{42}$ (55, 56).

By contrast, HDX of $A\beta_{42}$ showed an appreciable increase in protection by a modified sigmoidal behavior (Fig. 2, solid line; raw HDX data shown in Figs. S2–S5). The first stage is rapid and exponential-like, showing a rapid increase in protection. A first plateau follows wherein no significant change occurs in protection. A second increase in protection appears as a sigmoidal upward break in the curve, followed by a second plateau, indicating that the system reaches equilibrium among all of the species. The HMW species correspond to $A\beta_{42}$ soluble aggregates that concentrate upon centrifugation to the bottom-half solution. Importantly, these results are consistent with native gel and Western blotting that show formation of HMW $A\beta_{42}$ soluble species on the same time scale as the pulsed HDX experiments (Fig. 2, *Right*, lane 1).

We attribute the first rapid increase in the protection level to formation of small $A\beta_{42}$ oligomers (dimer, trimer, and tetramer, etc.), in line with previous work (34, 57). The plateau that follows indicates no additional significant hydrogen-bond formation or conformational change. During this stage, larger oligomers are forming with little increase in protection as $A\beta_{42}$ molecules add to the large soluble aggregates. After some time, the oligomers do reorganize, in an autocatalytic fashion, to a structure showing higher protection. The upward-breaking sigmoidal curve represents this reorganization and is consistent with the behavior of other amyloid-like proteins (i.e., they undergo nucleation, growth, and stabilization) (51). Whereas the rate of nucleation is slow, giving nearly constant HDX, the growth rate is much faster, giving the sigmoidal behavior of HDX. Similar sigmoidal behavior was reported recently for $A\beta_{42}$ aggregation followed by a fluorescent tetramethylrhodamine-labeled $A\beta_{42}$ derivative (57). Our approach has an advantage in that it can be used directly without the need for adding amino acids or fluorophores to the protein.

Application of Finke–Watzky Modeling and Statistical Evaluation by a Bootstrap Strategy. Amyloid-like proteins usually undergo a self-catalyzed aggregation process, which involves one nucleation step and one growth step. Although there are many models to describe a slow, continuous nucleation, we chose the simplest one to fit the time-dependent aggregation of $A\beta_{42}$ (Fig. 2), following the recommendation of Finke and coworkers (51). We modified the Finke–Watzky (F–W) model by adding a "dimerization" process (Eq. **1**). The model describes a reaction that proceeds from a monomer Aβ in state A to a "dimer" in state B (Eqs. **1–3**). Admittedly, state B, consisting of a heterogeneous mix of small oligomers, is more complicated than can be addressed in this modified F–W model. Nevertheless, considering it as dimer, we subsequently allowed its transformation to state C by nucleation of large, soluble oligomers, heterogeneous in structure and number. The model includes a forward rate constant k_1 of oligomerization, a rate constant k_{-1} for the reverse reaction, a forward nucleation rate constant k_2 from B to C, and a forward self-catalysis rate constant k_3 involving B and C. A useful parameter that can allow for a direct comparison of different aggregation curves is $t_{1/2}$, which is the time point at which the number of Aβ molecules in state C equals the remaining Aβ molecules.

$$A + A \underset{k_{-1}}{\overset{k_1}{\rightleftharpoons}} B \qquad [1]$$

$$B \xrightarrow{k_2} C \qquad [2]$$

$$B + C \xrightarrow{k_3} 2C \qquad [3]$$

In fitting the data to the F–W model, we sought a single parameter to characterize the outcome. The $t_{1/2}$ value is likely that parameter, and it could be obtained by averaging the $t_{1/2}$ values from three determinations. However, to obtain a better measure and use the full statistical value of the data, we evaluated the statistics by using a bootstrap resampling strategy. This gives a more reliable $t_{1/2}$ along with its precision, permitting the use

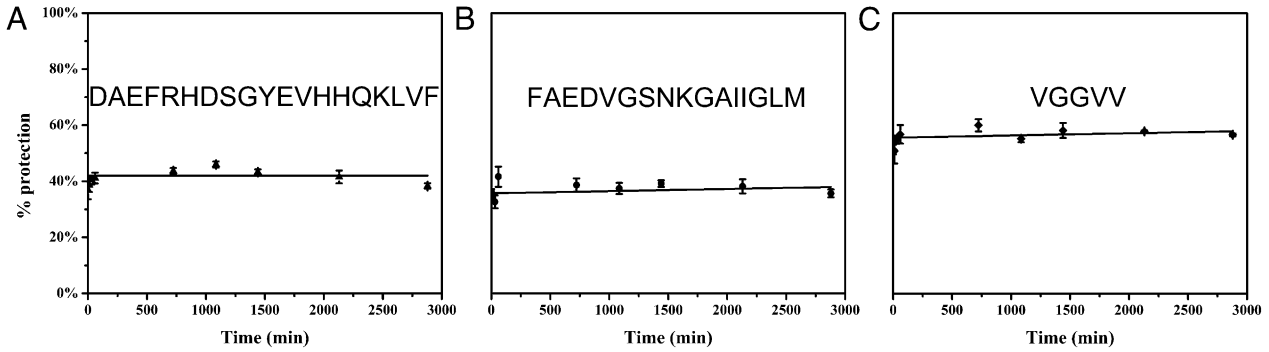

Fig. 1. Pulsed HDX results for three peptides from $A\beta_{40}$. Aggregation was done at 25 °C and in the absence of Cu^{2+}. Peptic peptides 1–19 (*A*), 20–35 (*B*), and 36–40 (*C*) are represented by triangles, circles, and diamonds, respectively. Lines were fit by using "linear fit" in OriginPro 8.5.

of a simple *t* test for establishing differences. By applying the bootstrap strategy (*Supporting Information*) to the F–W model (52–54) (Fig. 3 and Fig. S6), we retrieved not only $t_{1/2}$ values, but also rate-constant information and precision. Although there are many families of k_{-1}, k_1, k_2, and k_3 values that fit the experimental data, they are highly correlated (i.e., an increase in k_2 and a commensurate decrease in k_3 gives a good fit to the model). There is, however, a nearly constant $t_{1/2}$ for all of the fits for one peptide. More importantly, the $t_{1/2}$ values corresponding to the three peptides are different. The middle region (i.e., 20–35) has the shortest $t_{1/2}$ (1,070 ± 30 min), whereas C-terminus (i.e., 36–42) and N-terminus (i.e., 1–19) regions have longer $t_{1/2}$ values (1,230 ± 30 min and 1,420 ± 20 min, respectively; Fig. S7). That these differences among the three peptides are statistically significant is supported by the *t* test at ≥99.99% confidence level, made possible by using the bootstrap strategy. Although it may be surprising that the outcome treats the three peptides as separate entities, we note that proteins are complex species and give, for example, different HDX rate constants for different regions. These results now establish that the middle region (i.e., residues 20–35) is the first to report entering an organized state. This is consistent with most molecular dynamics simulations that point to the middle region as either a folding nucleus or a dimerization interface (58–60). The hinge region identified in the solid-state NMR results for $A\beta_{42}$ fibrils is from S26 to I31 (28), which lies in the middle of the region we identified here. This smaller region may also be important in initiating aggregation, as suggested by aggregation studies of myriad mutation forms. For example, Flemish (A21G) (61), Arctic (E22G) (62), Dutch (E22Q) (61, 63), Iowa (D23N) (64), and others (65) exhibit different aggregation behavior compared with the wild-type $A\beta_{42}$, supporting that the middle region of Aβ is important in the aggregation process.

The C terminus (residues 36–42) aggregates second, confirming that it plays a smaller but still important role in aggregation (49). All of the residues in this region (i.e., VGGVVIA) are hydrophobic, serving as an interface for $A\beta_{42}$ aggregation. Besides, the only differences between $A\beta_{40}$ and $A\beta_{42}$ are the last two residues of this region (i.e., IA) of $A\beta_{42}$.The strong differences in aggregation between $A\beta_{40}$ and $A\beta_{42}$ hint at the importance of the hydrophobic interaction within this region. As a result, we propose that without the last two residues the hydrophobic interaction would be insufficient to "pull" small aggregates together and form larger aggregates.

The N terminus (residues 1–19) aggregates last, consistent with its hydrophilic nature. Unlike other approaches showing that the N terminus is flexible (28), our data show some ordering in this region, and as expected, it is the last involved in the aggregation process. The observation that mice never develop AD, however, may be consistent with the importance of the N terminus, because the three mutations between mouse vs. human Aβ represent amino acid substitutions in this region (i.e., R5G, Y10F, and H13R). Nevertheless, the N terminus is involved in aggregation, and this might be the cause for the structural difference between soluble Aβ aggregates and insoluble Aβ fibrils. In addition, the structural difference may be relevant to the different levels of neurotoxicity exhibited by soluble Aβ aggregates vs. insoluble fibrils. Thus, these pulsed HDX studies should have an important impact in the design of drugs that can alter the aggregation of Aβ species and ultimately their neurotoxicity.

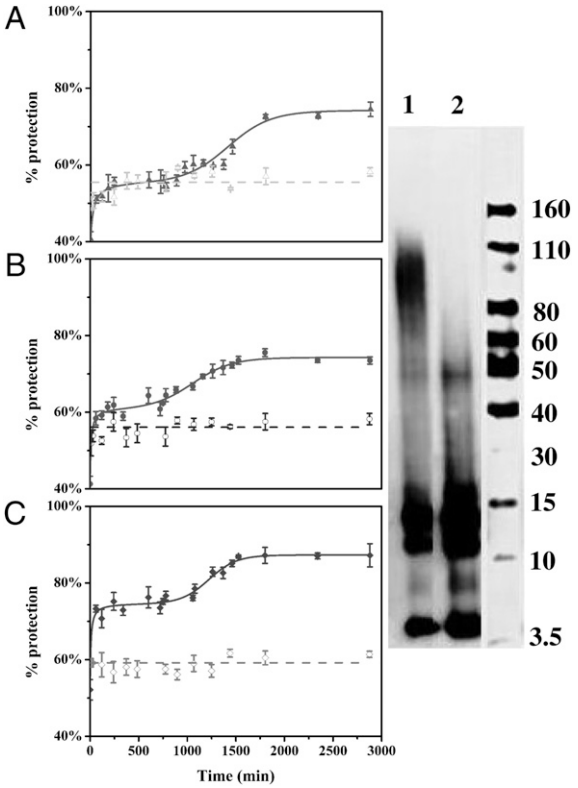

Fig. 2. Pulsed HDX (*Left*) and Western blotting (*Right*) results for three peptic peptides from $A\beta_{42}$. Aggregation was done at 25 °C and in the absence (solid triangles, circles, and diamonds) or presence of Cu^{2+} (hollow triangles, circles, and diamonds). Peptic peptides 1–19 (*A*), 20–35 (*B*), and 36–42 (*C*) are represented by triangles, circles, and diamonds, respectively. Dashed lines are fits using "linear fit" in OriginPro 8.5. Solid lines are fits using a modified F–W model in Mathcad. Native gel and Western blotting of the aggregated $A\beta_{42}$ samples (incubated at 25 °C for 48 h), in the absence (lane 1) or presence of Cu^{2+} (lane 2).

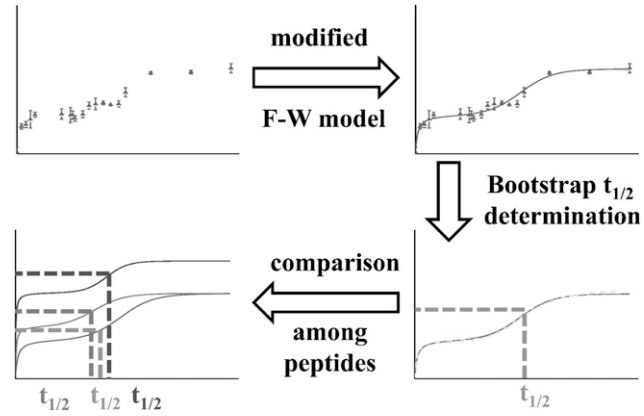

Fig. 3. Flowchart for the modified F–W modeling and bootstrap strategy.

Pulsed HDX Analysis of $A\beta_{42}$ Fibrils. Even though the liquid chromatography (LC)–MS/MS identification showed full coverage for the peptides, there was some undigested $A\beta_{42}$ observed as monomer mass in the above experiments, and its corresponding relative peak intensity increased with increasing incubation time. Our online pepsin digestion has been tested in many other projects (66, 67), and the digestion efficiency approaches 100% for proteins, most of which are larger than $A\beta_{42}$. The $A\beta_{42}$ peptide showed the lowest digestion efficiency, suggesting the presence of amyloid fibrils or other HMW aggregates that are slow to proteolyze. The protection levels of these undigested species (Fig. S8*A*) are higher than that of $A\beta_{42}$ species that can undergo pepsin proteolysis. Given that we observed no significant peaks corresponding to the monomeric mass of $A\beta_{40}$ in its aggregation experiments, the result for $A\beta_{42}$ is further evidence that the amyloid fibrils are the source of peaks representing undigested $A\beta_{42}$.

To study directly the amyloid fibrils, we applied pulsed HDX to the preformed $A\beta_{42}$ fibrils, which represent the final stage of Aβ aggregation. Digestion of amyloid fibrils is difficult (31, 68) and usually requires the use of "strong" chemicals including hexafluoroisopropanol or DMSO to dissociate all aggregates into $A\beta_{42}$ monomer (49). This time-consuming and MS-unfriendly digestion protocol is not suitable for an HDX platform. We tested the effectiveness of the HDX quenching procedure (3 M urea with 1% TFA) by using transmission EM and found the protocol was able to dissociate to some extent the amyloid fibrils, allowing us to measure the HDX of the fibrils (Fig. S9).

Upon pulsed HDX of the preformed fibrils we observed both the peptides formed by pepsin digestion (i.e., 1–19) and the undigested $A\beta_{42}$. The peptides and the full $A\beta_{42}$ are similarly protected (89 ± 1% for the undigested $A\beta_{42}$ and 85 ± 1%, 84 ± 1%, and 91 ± 2% for 1–19, 20–35 and 36–42, respectively), consistent with the peptides' being proteolytic fragments from the amyloid fibrils. This conclusion is consistent with a study that shows the recycling mechanism of $A\beta_{42}$ fibrils with the $A\beta_{42}$ monomer (45). The monomer thus formed carries information of the "imprinted" fibrils because quenching HDX preserves information before MS analysis. These monomers digest well with pepsin owing to a lack of the highly packed structure characteristic of the amyloid fibrils. Thus, the peptide fragments are useful "fibril reporters" because they contain the same protection as their precursor fibrils. These amyloid fibrils, which become ultimately the main component in the incubation, are considerably more difficult to interrogate because they have a highly compact structure. Nevertheless, the highly organic mobile phase we used is sufficient to denature some of the fibrils and release detectable amounts of $A\beta_{42}$ monomer (31). The protection level of undigested $A\beta_{42}$ seen in the previously mentioned experiments (Fig. S8*A*) is similar to that of the preformed fibrils, both digested and undigested, indicating that the full $A\beta_{42}$ peptide originates from the $A\beta_{42}$ fibrils whereas the peptic peptides arise from soluble species.

To rule out a significant contribution of undigested $A\beta_{42}$ to our time-dependent studies described earlier, we measured directly the digestion of amyloid fibrils by examining the relative peak-area ratios in extracted ion chromatograms (EICs) of the peptide fragments and the undigested $A\beta_{42}$. We used the N-terminal region (i.e., 1–19) as a measure of fibril digestion, and the ratio of its EIC peak area compared with that of the undigested $A\beta_{42}$ is 0.078, indicating that only a small fraction of fibrils undergo digestion. Thus, the contribution of fibril digestion to the peptide-fragment signals is likely small because the peptide 1–19 signal area in the EIC was considerably greater than the EIC area corresponding to the undigested protein (discussed below). Because HDX reports an ensemble average, the protection levels seen in the digested peptides are a measure of soluble $A\beta_{42}$ aggregates, rather than of the insoluble Aβ species.

Pulsed HDX Analysis of Factors Affecting $A\beta_{42}$ Aggregation. One motivation for the HDX pulsed platform is to develop a tool to investigate the many factors that affect $A\beta_{42}$ oligomerization and aggregation (and of other amyloid-forming proteins). Such a platform should rapidly provide insight on those factors that affect $A\beta_{42}$ aggregation. Shifts in or losses of the sigmoidal behavior are a measure of the effect. One factor of high interest to us is

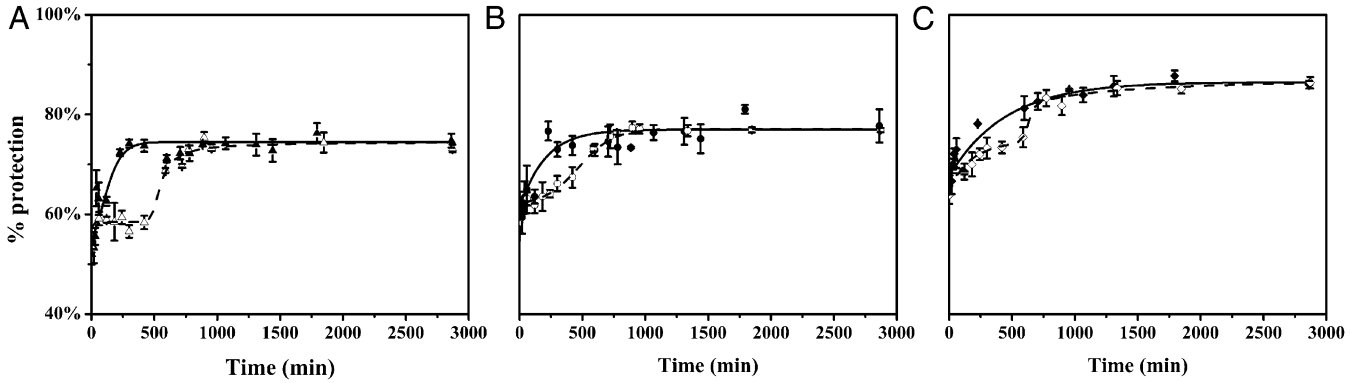

Fig. 4. Pulsed HDX results for three peptides from $A\beta_{42}$. Aggregation was done at 37 °C, with agitation at 150 rpm and in the absence (solid triangles, circles, and diamonds) or presence of Cu^{2+} (hollow triangles, circles, and diamonds). Peptic peptides 1–19 (*A*), 20–35 (*B*), and 36–42 (*C*) are represented by triangles, circles, and diamonds, respectively. Solid lines are fits using a simple F–W model and dashed lines are fits using a modified F–W model in Mathcad.

that of Cu^{2+}, which has been previously implicated in $A\beta_{42}$ aggregation (14, 18, 19). Thus, we added Cu^{2+} to the PBS buffer before mixing with $A\beta_{42}$ such that the final stoichiometry of Cu^{2+} and $A\beta_{42}$ is 1:1 (molar ratio). The pulsed HDX results of $A\beta_{42}$ incubation in the absence of Cu^{2+} provide the reference point for this experiment. The protection level of $A\beta_{42}$ incubated with Cu^{2+} is remarkably linear and unchanged for the three peptic peptides (i.e., 1–19, 20–35, and 36–42; Fig. 2, dashed lines; raw data shown in Fig. S3), in contrast to their sigmoidal behavior in the absence of Cu^{2+} (Fig. 2, solid lines; raw data shown in Fig. S2). The plateau stage of protection in the presence of Cu^{2+} is similar to that represented by the first plateau for 1–19 in the absence of Cu^{2+} (55%). The protection is lower than that of both 20–35 and 36–42 (56% vs. 60% and 60% vs. 75%, respectively).

We hypothesize that the differences of protection in the presence and absence of Cu^{2+} is that Cu^{2+} stabilizes different forms of Aβ aggregates by interacting with them. The coordination sites for Cu^{2+} are likely on the N terminus (i.e., H6, H13, and H14) (14, 17), and coordination to these sites would lead to more protection of that region of $A\beta_{42}$. By contrast, the hydrophobic interactions between the C termini of Aβ peptides may be diminished to compensate for the Cu^{2+} coordination. In addition, native gel and Western blotting of the samples corresponding to the largest difference on the pulsed HDX curve show much less HMW soluble aggregates (50–110 kDa) and more LMW aggregates (i.e., mainly trimer and tetramer) in the presence vs. absence of Cu^{2+} (Fig. 2, *Right*). This result reinforces our previous report showing that Cu^{2+} stabilizes the soluble $A\beta_{42}$ aggregates and inhibits formation of amyloid fibrils (14, 19).

We also tested the ability of our pulsed HDX approach under rapidly aggregating conditions such as higher temperature and with agitation. We chose a higher and more physiologically relevant temperature (37 °C) and agitated the solution (at 150 rpm, Fig. 4, solid line; raw data shown in Fig. S4). Compared with the results at 25 °C in the absence of Cu^{2+} and without agitation, the aggregation behavior speeded up considerably. The lag phase disappears, indicating that the transformation from LMW aggregates to HMW aggregates is expedited. Next, we repeated the experiment at higher temperature and subjected the solution to agitation, as well as added Cu^{2+} to the solution. According to the results just discussed, applying higher temperature and agitation should decrease the lag phase of $A\beta_{42}$ aggregation, whereas Cu^{2+} should slow down the aggregation. Indeed, the results (Fig. 4, dashed line; raw data shown in Fig. S5) indicate that the $A\beta_{42}$ aggregation is faster than that at 25 °C, yet a lag phase is observed in the presence of Cu^{2+}. This agrees with the hypothesis that higher temperature and agitation accelerate the aggregation. However, the results showed slower kinetics than that for $A\beta_{42}$ aggregation at 37 °C, 150 rpm, in the absence of Cu^{2+}, providing evidence that Cu^{2+} slows down the $A\beta_{42}$ aggregation, even at 37 °C, yet without completely preventing it.

As we observed in experiments of $A\beta_{42}$ incubated at 25 °C, the peaks corresponding to the $A\beta_{42}$ monomer (undigested species) were observed in all experiments mentioned in this section. The extent of protection of the corresponding undigested species is higher than observed for peptide fragments in the same experiments, and similar to those of both digested and undigested preformed fibrils (Fig. S8 *B–D*).

The ratios of peak intensities corresponding to $A\beta_{42}$ that can be digested relative to that resistant to digestion now range from 17 to 1.1. After longer incubation times, more and more $A\beta_{42}$ becomes resistant to digestion. These ratios are 210 to 14 times higher than the ratio calculated from preformed fibrils described above (i.e., 0.078), indicating that only a very small amount of the fibrils was digested and thus is not expected to interfere to a large extent with the protection levels calculated from these experiments. Importantly, this result indicates that our platform reports only on the soluble Aβ species and not insoluble aggregates.

Conclusion

A new implementation of the pulsed HDX technique interfaced with LC/MS provides an opportunity to examine the details of aggregation of the Aβ peptide at various stages. By using this method, we successfully decoupled the aggregation from the HDX process. Importantly, we extracted kinetic information on the $A\beta_{42}$ aggregation at 25 °C, indicating that the middle region of the $A\beta_{42}$ peptide (i.e., 20–35) was the "seeding" region in aggregation, followed by the C-terminus hydrophobic region (i.e., 36–42) and then the N-terminus hydrophilic region (i.e., 1–19). Finally, we showed that this approach allowed us to examine directly the factors that affect the oligomerization of $A\beta_{42}$. For example, at 37 °C and with agitation, $A\beta_{42}$ aggregated faster than at 25 °C. To the contrary, the presence of Cu^{2+} slowed down the $A\beta_{42}$ aggregation, presumably by complexing the polypeptide in the N-terminal region and stabilizing the soluble $A\beta_{42}$ species.

We envision this approach as a general tool to support future efforts to measure rates of $A\beta_{42}$ oligomerization and aggregation as a function of various parameters (e.g., concentration, presence of different ligands or proteins, and pH). We also see the need for more effort in using MS site-specific ion activation (i.e., electron-transfer dissociation) to obtain information at the amino acid level and probe in more detail the aggregation interface and the Cu^{2+} binding sites. Alternative footprinting approaches including fast photochemical oxidation may also offer complementary views to understand amyloid formation. Moreover, the method described herein is applicable to the study of various experimental conditions on the oligomerization and aggregation of other amyloid-forming proteins involved in neurodegenerative diseases.

ACKNOWLEDGMENTS. We acknowledge helpful discussions and support from Prof. Carl Frieden and Dr. Kanchan Garai. L.M.M. acknowledges generous financial support from the Oak Ridge Associated Universities for a Ralph E. Powe Junior Faculty Award, the Washington University Knight Alzheimer's Disease Research Center (National Institutes of Health Grant P50-AG05681), and Alzheimer's Association Grant NIRP-12-259199. This research was supported by National Institute of General Medical Sciences Grant 8 P41 GM103422-35 of the National Institutes of Health (to M.L.G.).

1. Roher AE, et al. (1993) beta-Amyloid-(1-42) is a major component of cerebrovascular amyloid deposits: Implications for the pathology of Alzheimer disease. *Proc Natl Acad Sci USA* 90(22):10836–10840.
2. Jarrett JT, Berger EP, Lansbury PT, Jr. (1993) The carboxy terminus of the beta amyloid protein is critical for the seeding of amyloid formation: Implications for the pathogenesis of Alzheimer's disease. *Biochemistry* 32(18):4693–4697.
3. Fagan AM, Holtzman DM (2010) Cerebrospinal fluid biomarkers of Alzheimer's disease. *Biomarkers Med* 4(1):51–63.
4. Kim J, et al. (2011) Haploinsufficiency of human APOE reduces amyloid deposition in a mouse model of amyloid-β amyloidosis. *J Neurosci* 31(49):18007–18012.
5. McGowan E, et al. (2005) Abeta42 is essential for parenchymal and vascular amyloid deposition in mice. *Neuron* 47(2):191–199.
6. Kim J, et al. (2007) Abeta40 inhibits amyloid deposition in vivo. *J Neurosci* 27(3):627–633.
7. Pauwels K, et al. (2012) Structural basis for increased toxicity of pathological aβ42: aβ40 ratios in Alzheimer disease. *J Biol Chem* 287(8):5650–5660.
8. Klein WL, Stine WB, Jr., Teplow DB (2004) Small assemblies of unmodified amyloid beta-protein are the proximate neurotoxin in Alzheimer's disease. *Neurobiol Aging* 25(5):569–580.
9. Cleary JP, et al. (2005) Natural oligomers of the amyloid-beta protein specifically disrupt cognitive function. *Nat Neurosci* 8(1):79–84.
10. Lesné S, et al. (2006) A specific amyloid-beta protein assembly in the brain impairs memory. *Nature* 440(7082):352–357.
11. Bharadwaj PR, Dubey AK, Masters CL, Martins RN, Macreadie IG (2009) Abeta aggregation and possible implications in Alzheimer's disease pathogenesis. *J Cell Mol Med* 13(3):412–421.
12. Masuda Y, et al. (2009) Identification of physiological and toxic conformations in Abeta42 aggregates. *ChemBioChem* 10(2):287–295.
13. Upadhaya AR, Lungrin I, Yamaguchi H, Fändrich M, Thal DR (2012) High-molecular weight Aβ oligomers and protofibrils are the predominant Aβ species in the native soluble protein fraction of the AD brain. *J Cell Mol Med* 16(2):287–295.

14. Atwood CS, et al. (1998) Dramatic aggregation of Alzheimer abeta by Cu(II) is induced by conditions representing physiological acidosis. *J Biol Chem* 273(21):12817–12826.
15. Atwood CS, et al. (2004) Copper mediates dityrosine cross-linking of Alzheimer's amyloid-beta. *Biochemistry* 43(2):560–568.
16. Tõugu V, et al. (2009) Zn(II)- and Cu(II)-induced non-fibrillar aggregates of amyloid-beta (1-42) peptide are transformed to amyloid fibrils, both spontaneously and under the influence of metal chelators. *J Neurochem* 110(6):1784–1795.
17. Alí-Torres J, Maréchal JD, Rodríguez-Santiago L, Sodupe M (2011) Three dimensional models of Cu(2+)-Aβ(1-16) complexes from computational approaches. *J Am Chem Soc* 133(38):15008–15014.
18. García S, et al. (2012) Dual role of Cu^{2+} ions on the aggregation and degradation of soluble Aβ oligomers and protofibrils investigated by fluorescence spectroscopy and AFM. *J Inorg Biochem* 116:26–36.
19. Sharma AK, et al. (2012) Bifunctional compounds for controlling metal-mediated aggregation of the aβ42 peptide. *J Am Chem Soc* 134(15):6625–6636.
20. Gong Y, et al. (2003) Alzheimer's disease-affected brain: Presence of oligomeric A beta ligands (ADDLs) suggests a molecular basis for reversible memory loss. *Proc Natl Acad Sci USA* 100(18):10417–10422.
21. Prohaska JR, Gybina AA (2004) Intracellular copper transport in mammals. *J Nutr* 134(5):1003–1006.
22. Sawaya MR, et al. (2007) Atomic structures of amyloid cross-beta spines reveal varied steric zippers. *Nature* 447(7143):453–457.
23. Laganowsky A, et al. (2012) Atomic view of a toxic amyloid small oligomer. *Science* 335(6073):1228–1231.
24. Stroud JC, Liu C, Teng PK, Eisenberg D (2012) Toxic fibrillar oligomers of amyloid-β have cross-β structure. *Proc Natl Acad Sci USA* 109(20):7717–7722.
25. Castaño EM, et al. (1986) In vitro formation of amyloid fibrils from two synthetic peptides of different lengths homologous to Alzheimer's disease beta-protein. *Biochem Biophys Res Commun* 141(2):782–789.
26. Miller Y, Ma B, Tsai CJ, Nussinov R (2010) Hollow core of Alzheimer's Abeta42 amyloid observed by cryoEM is relevant at physiological pH. *Proc Natl Acad Sci USA* 107(32): 14128–14133.
27. LeVine H, 3rd (1999) Quantification of beta-sheet amyloid fibril structures with thioflavin T. *Methods Enzymol* 309:274–284.
28. Lührs T, et al. (2005) 3D structure of Alzheimer's amyloid-beta(1-42) fibrils. *Proc Natl Acad Sci USA* 102(48):17342–17347.
29. Fawzi NL, Ying J, Ghirlando R, Torchia DA, Clore GM (2011) Atomic-resolution dynamics on the surface of amyloid-β protofibrils probed by solution NMR. *Nature* 480(7376):268–272.
30. Parthasarathy S, et al. (2011) Molecular-level examination of Cu2+ binding structure for amyloid fibrils of 40-residue Alzheimer's β by solid-state NMR spectroscopy. *J Am Chem Soc* 133(10):3390–3400.
31. Kheterpal I, Zhou S, Cook KD, Wetzel R (2000) Abeta amyloid fibrils possess a core structure highly resistant to hydrogen exchange. *Proc Natl Acad Sci USA* 97(25): 13597–13601.
32. Kheterpal I, et al. (2003) Abeta protofibrils possess a stable core structure resistant to hydrogen exchange. *Biochemistry* 42(48):14092–14098.
33. Carulla N, Zhou M, Giralt E, Robinson CV, Dobson CM (2010) Structure and intermolecular dynamics of aggregates populated during amyloid fibril formation studied by hydrogen/deuterium exchange. *Acc Chem Res* 43(8):1072–1079.
34. Bernstein SL, et al. (2009) Amyloid-β protein oligomerization and the importance of tetramers and dodecamers in the aetiology of Alzheimer's disease. *Nat Chem* 1(4): 326–331.
35. Zheng X, et al. (2012) Z-Phe-Ala-diazomethylketone (PADK) disrupts and remodels early oligomer states of the Alzheimer disease Aβ42 protein. *J Biol Chem* 287(9): 6084–6088.
36. Gessel MM, et al. (2012) Aβ(39-42) modulates Aβ oligomerization but not fibril formation. *Biochemistry* 51(1):108–117.
37. Chalmers MJ, et al. (2006) Probing protein ligand interactions by automated hydrogen/deuterium exchange mass spectrometry. *Anal Chem* 78(4):1005–1014.
38. Kaltashov IA, Bobst CE, Abzalimov RR (2009) H/D exchange and mass spectrometry in the studies of protein conformation and dynamics: Is there a need for a top-down approach? *Anal Chem* 81(19):7892–7899.
39. Zhang J, et al. (2010) Hydrogen/deuterium exchange reveals distinct agonist/partial agonist receptor dynamics within vitamin D receptor/retinoid X receptor heterodimer. *Structure* 18(10):1332–1341.
40. Chalmers MJ, Busby SA, Pascal BD, West GM, Griffin PR (2011) Differential hydrogen/deuterium exchange mass spectrometry analysis of protein-ligand interactions. *Expert Rev Proteomics* 8(1):43–59.
41. Zhang Z, Smith DL (1993) Determination of amide hydrogen exchange by mass spectrometry: a new tool for protein structure elucidation. *Protein Sci* 2(4):522–531.
42. Wales TE, Engen JR (2006) Hydrogen exchange mass spectrometry for the analysis of protein dynamics. *Mass Spectrom Rev* 25(1):158–170.
43. Pan J, Han J, Borchers CH, Konermann L (2011) Conformer-specific hydrogen exchange analysis of Aβ(1-42) oligomers by top-down electron capture dissociation mass spectrometry. *Anal Chem* 83(13):5386–5393.
44. Pan J, Han J, Borchers CH, Konermann L (2012) Structure and dynamics of small soluble Aβ(1-40) oligomers studied by top-down hydrogen exchange mass spectrometry. *Biochemistry* 51(17):3694–3703.
45. Sánchez L, et al. (2011) Aβ40 and Aβ42 amyloid fibrils exhibit distinct molecular recycling properties. *J Am Chem Soc* 133(17):6505–6508.
46. Roder H, Elöve GA, Englander SW (1988) Structural characterization of folding intermediates in cytochrome c by H-exchange labelling and proton NMR. *Nature* 335(6192):700–704.
47. Pan J, Wilson DJ, Konermann L (2005) Pulsed hydrogen exchange and electrospray charge-state distribution as complementary probes of protein structure in kinetic experiments: implications for ubiquitin folding. *Biochemistry* 44(24):8627–8633.
48. Khanal A, Pan Y, Brown LS, Konermann L (2012) Pulsed hydrogen/deuterium exchange mass spectrometry for time-resolved membrane protein folding studies. *J Mass Spectrom* 47(12):1620–1626.
49. Dahlgren KN, et al. (2002) Oligomeric and fibrillar species of amyloid-beta peptides differentially affect neuronal viability. *J Biol Chem* 277(35):32046–32053.
50. Zhang Z, Marshall AG (1998) A universal algorithm for fast and automated charge state deconvolution of electrospray mass-to-charge ratio spectra. *J Am Soc Mass Spectrom* 9(3):225–233.
51. Morris AM, Watzky MA, Agar JN, Finke RG (2008) Fitting neurological protein aggregation kinetic data via a 2-step, minimal/"Ockham's razor" model: The Finke-Watzky mechanism of nucleation followed by autocatalytic surface growth. *Biochemistry* 47(8):2413–2427.
52. Caceci MS (1989) Estimating error limits in parametric curve fitting. *Anal Chem* 61(20): 2324–2327.
53. Efron B (1979) 1977 Rietz Lecture - Bootstrap methods - Another look at the jackknife. *Ann Stat* 7(1):1–26.
54. Efron B, Tibshirani R (1993) *An Introduction to the Bootstrap* (Chapman & Hall, New York), p xvi.
55. Murray MM, et al. (2009) Amyloid beta protein: Abeta40 inhibits Abeta42 oligomerization. *J Am Chem Soc* 131(18):6316–6317.
56. Yan Y, Wang C (2007) Abeta40 protects non-toxic Abeta42 monomer from aggregation. *J Mol Biol* 369(4):909–916.
57. Garai K, Frieden C (2013) Quantitative analysis of the time course of Aβ oligomerization and subsequent growth steps using tetramethylrhodamine-labeled Aβ. *Proc Natl Acad Sci USA* 110(9):3321–3326.
58. Urbanc B, Betnel M, Cruz L, Bitan G, Teplow DB (2010) Elucidation of amyloid beta-protein oligomerization mechanisms: Discrete molecular dynamics study. *J Am Chem Soc* 132(12):4266–4280.
59. Cruz L, Rao JS, Teplow DB, Urbanc B (2012) Dynamics of metastable β-hairpin structures in the folding nucleus of amyloid β-protein. *J Phys Chem B* 116(22):6311–6325.
60. Roychaudhuri R, Yang M, Condron MM, Teplow DB (2012) Structural dynamics of the amyloid β-protein monomer folding nucleus. *Biochemistry* 51(19):3957–3959.
61. Kumar-Singh S, et al. (2002) In vitro studies of Flemish, Dutch, and wild-type beta-amyloid provide evidence for two-staged neurotoxicity. *Neurobiol Dis* 11(2):330–340.
62. Nilsberth C, et al. (2001) The 'Arctic' APP mutation (E693G) causes Alzheimer's disease by enhanced Abeta protofibril formation. *Nat Neurosci* 4(9):887–893.
63. Levy E, et al. (1990) Mutation of the Alzheimer's disease amyloid gene in hereditary cerebral hemorrhage, Dutch type. *Science* 248(4959):1124–1126.
64. Grabowski TJ, Cho HS, Vonsattel JP, Rebeck GW, Greenberg SM (2001) Novel amyloid precursor protein mutation in an Iowa family with dementia and severe cerebral amyloid angiopathy. *Ann Neurol* 49(6):697–705.
65. Murakami K, et al. (2002) Synthesis, aggregation, neurotoxicity, and secondary structure of various A beta 1-42 mutants of familial Alzheimer's disease at positions 21-23. *Biochem Biophys Res Commun* 294(1):5–10.
66. Zhang J, Ramachandran P, Kumar R, Gross ML (2013) H/D exchange centroid monitoring is insufficient to show differences in the behavior of protein states. *J Am Soc Mass Spectrom* 24(3):450–453.
67. Huang RY, Garai K, Frieden C, Gross ML (2011) Hydrogen/deuterium exchange and electron-transfer dissociation mass spectrometry determine the interface and dynamics of apolipoprotein E oligomerization. *Biochemistry* 50(43):9273–9282.
68. Stine WB, Jr., Dahlgren KN, Krafft GA, LaDu MJ (2003) In vitro characterization of conditions for amyloid-beta peptide oligomerization and fibrillogenesis. *J Biol Chem* 278(13):11612–11622.